

# FPGA-based $\alpha/\gamma$ pulse shape discrimination for BaF<sub>2</sub> detector using 2-GSPS fast waveform sampling

Chen-Fei Yang<sup>1,2</sup> · Chang-Qing Feng<sup>1,2</sup> · Shu-Bin Liu<sup>1,2</sup> · Qi An<sup>1,2</sup>

Received: 28 May 2016/Revised: 16 August 2016/Accepted: 22 August 2016/Published online: 24 December 2016  
© Shanghai Institute of Applied Physics, Chinese Academy of Sciences, Chinese Nuclear Society, Science Press China and Springer Science+Business Media Singapore 2016

**Abstract** Four FPGA-based  $\alpha/\gamma$  pulse shape discrimination algorithms for BaF<sub>2</sub> detector are investigated and compared in this paper. A 2-GSPS fast waveform sampling board based on DRS4 chip is employed to sample the pulses. The test results with a <sup>22</sup>Na  $\gamma$ -source and the natural radioactivity of BaF<sub>2</sub> show good discrimination performance of the algorithms, with false rates around 1%. Small logical resource occupancy and short dead time are achieved. About 4400 slices are used in FPGA for pulse sampling and real-time discrimination altogether.

**Keywords** BaF<sub>2</sub> · Pulse extraction ·  $\alpha/\gamma$  Discrimination · DRS4 · FPGA

## 1 Introduction

Since the discovery of the intense, fast component of light pulse from BaF<sub>2</sub> crystal in 1980s [1], BaF<sub>2</sub> scintillators have been extensively used in nuclear physics and elementary-particle physics for detecting  $\gamma$ -rays and light charged particles [2, 3], especially in medium and high energy regions.

Commonly, BaF<sub>2</sub> crystals contain radium impurity, leading to background constituted mainly by  $\alpha$ -particles and in minor extent by  $\gamma$ -rays and electrons [4]. The possibility of discriminating particles from  $\gamma$ -rays and rejecting the background is an important issue in  $\gamma$ -spectroscopy. The radioluminescence spectrum of BaF<sub>2</sub> crystal contains a fast component with an extremely short decay time of 0.6 ns and a slow component with decay time of 620 ns. The fast/slow component ratio is large for  $\gamma$ -rays and small for heavy particles [5–7]. This allows one to discriminate heavy particles (such as  $\alpha$ -particles) from  $\gamma$ -rays. Traditionally, analog methods were used for discrimination, with complex circuits and long dead times [8, 9]. Over the past decade, with the advancement of electronics and digital signal processing technology, digital pulse shape discrimination techniques are extensively used [2, 9]. To date, most works used ADCs for signal digitalization and executed the digital algorithms by software, which would limit the processing speed.

In this paper, we discuss four digital  $\alpha/\gamma$  pulse shape discrimination (PSD) algorithms for BaF<sub>2</sub> scintillator, using 2-GSPS (gigasamples per second) fast waveform sampling and FPGA-based pulse information extraction. The DRS4, a switched capacitor arrays chip, is used for waveform sampling. The PSD algorithms are compared utilizing the natural radioactivity of BaF<sub>2</sub> crystal and a <sup>22</sup>Na  $\gamma$ -ray source.

## 2 Digital signal processing of pulses

Caused by the light quenching effect in BaF<sub>2</sub> crystal, the fast/slow component ratio is greater for  $\gamma$ -induced pulse than  $\alpha$ -induced pulse. Figure 1 shows two waveforms from

---

This work was supported by the National Natural Science Foundation of China (No. 11205154).

---

✉ Chang-Qing Feng  
fengcq@ustc.edu.cn

<sup>1</sup> State Key Laboratory of Particle Detection and Electronics, University of Science and Technology of China, Hefei 230026, China

<sup>2</sup> Department of Modern Physics, University of Science and Technology of China, Hefei 230026, China

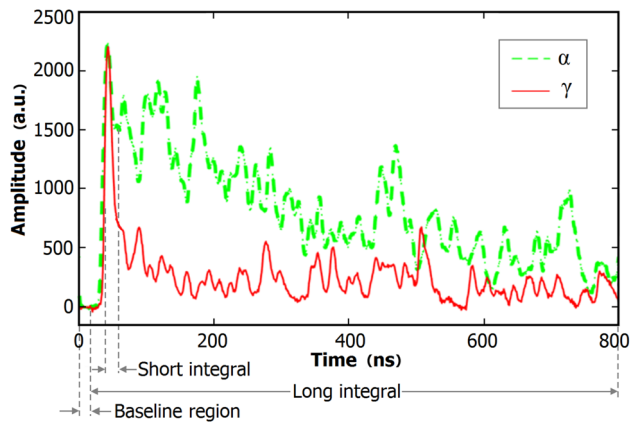


**Fig. 1** Typical signals from BaF<sub>2</sub> crystal, sampled at 2 GSPS. The regions for calculating long and short integrals and the baseline are indicated. (Color figure online)

a BaF<sub>2</sub> crystal: the green waveform from  $\alpha$ -particle and the red from  $\gamma$ -ray. The  $\alpha/\gamma$  PSD algorithms include the charge comparison method (CCM) [10], pulse peak analysis (PPA), pulse gradient analysis (PGA) [11] and finite impulse response filter comparison method (FCM).

## 2.1 Charge comparison method

The CCM is based on comparing the long and short integrals over different scales of one pulse. The long integral is a summation of the entire pulse samples, while the short integral is a summation of several samples near the maximum sample. In this paper, the optimum short integral is the summation of 16 samples: 5 samples before and 10 samples after the maximum sample, and the maximum sample itself. The regions for the long and short integrals are illustrated in Fig. 1. The short integral corresponds to the region of the fast component, while the long integral represents the sum of the fast and slow components. The  $\gamma$ -induced events, with larger fast/slow component ratios than the  $\alpha$ -induced events, should have larger short integrals for long integrals in the same length as those of the  $\alpha$ -induced events.

## 2.2 Pulse peak analysis

The PPA is based on comparing the long integral and amplitude of the maximum sample, i.e., peak of the pulse. As shown in Fig. 1, for the same peak amplitudes,  $\gamma$ -induced pulses have smaller long integrals than  $\alpha$ -induced pulses, due to larger fast/slow component ratios in BaF<sub>2</sub> scintillation.

## 2.3 Pulse gradient analysis

The PGA is based on comparing the long integral and the amplitude difference between the peak and the sample

occurring at a defined time interval after the peak. The amplitude difference is often referred as the discrimination gradient, and the specific sample's amplitude is known as the discrimination amplitude. The time interval was 5 ns in this work, considering different decay times of the fast and slow components and timing property of the photomultiplier tube (PMT). The decay time of the digitized fast component was 3–4 ns; therefore, the discrimination amplitude mainly depends on the amplitude of the slow component, while the peak mainly depends on amplitude of the fast component. Due to the larger fast/slow component ratios, the  $\gamma$ -induced events have bigger discrimination gradients for long integrals in same length as those of  $\alpha$ -induced events.

## 2.4 Finite impulse response filter comparison method (FCM)

Through frequency spectrum analysis, the fast components in BaF<sub>2</sub> pulses correspond to higher frequencies, at about 100 MHz, whereas the slow components are mostly lower than 2 MHz in the frequency domain. The pulses from BaF<sub>2</sub> crystal are processed by a FIR low-pass filter. A proper low-pass filter reduces the amplitude of fast component much more than that of the slow component. In this study, the passband frequency of 3 MHz was chosen for the filter after tests from 2 to 100 MHz. The filter output amplitude/filter input amplitude ratio of a  $\gamma$ -induced event, owing to its greater fast/slow component ratio, should be smaller than that of an  $\alpha$ -induced event. This ratio is called the FIR peak ratio.

## 2.5 Pulse information extraction

When sampling BaF<sub>2</sub> scintillation signal, the data rate is extremely high in consideration of the high sampling rate and high event rate ( $\sim 50$ – $200$  Hz, depending on the source activity). Instead of sending the raw pulse shapes (a 2080-byte package for each pulse) and analyzing the pulses in a computer as in most prior works, bad pulse elimination and pulse information extraction are executed in field programmable gate array (FPGA), and the pulse information (a 32-byte package for each pulse) is sent to a computer. This reduces the data transfer by 64 times. At the USB transfer rate of 20 MBps, the transmission time decreases to 1.6 from 100  $\mu$ s, which tremendously reduces the dead time correspondingly.

After digitization of the pulse, a simple baseline restorer algorithm is applied. The baseline value is calculated as the mean value of the first 16 samples, as shown in Fig. 1, and subtracted from the whole pulse form. Then, all the information needed for the four PSD methods is extracted from each pulse form, namely long integral, short integral,

peak amplitude, discrimination gradient and filter output amplitude. Figure 2 shows the flow of digital processing. Finally, together with packet flags, information of each pulse is sent to the computer through USB port as a 32-byte package.

### 3 Experimental setup and results

#### 3.1 Experimental setup

In this work, a cylindrical BaF<sub>2</sub> crystal of  $\Phi 5\text{ cm} \times 3\text{ cm}$  was instrumented with a XP2020Q PMT, and a collimated <sup>22</sup>Na source was placed 5 cm apart from it. The PMT was biased at  $-1.8\text{ kV}$ , which was considerably lower than the maximum rating value ( $-2.6\text{ kV}$ ). To verify the PSD algorithms, a NaI detector was placed opposite to BaF<sub>2</sub> detector for coincidence.

The PMT anodes were connected to inputs of a 2-GSPS fast sampling board based on a DRS4 chip [12], the fourth version of Domino Ring Sampler (DRS) from Paul Scherrer Institute (PSI), Switzerland. The sampling board was capable of sampling four independent input channels of 1024-cell sampling depth, and with 300 MHz sine wave input, the signal-to-noise and distortion ratio (SINAD) of this sampling board reached 39.7 dB, which corresponded to an effective number of bits (ENOB) of about 7 bits [13]. Using this sampling board, we achieved 7.5% energy resolution of the full-energy peak of <sup>22</sup>Na at 1.275 MeV. A low-end FPGA from Xilinx Spartan-3 family (XC3S5000) [14] was employed for digital signal processing on the sampling board. The experimental arrangement is shown schematically in Fig. 3.

#### 3.2 Results: natural background

As previously mentioned, a characteristic of BaF<sub>2</sub> crystals is the background caused by radium impurities constituted by  $\alpha$ -particles,  $\gamma$ -rays and electrons. Thus, we

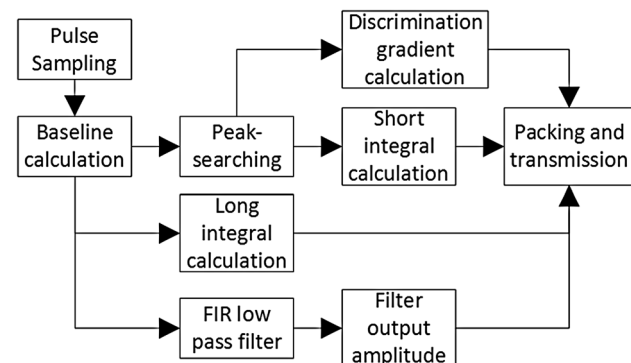


Fig. 2 Digital signal processing flowchart

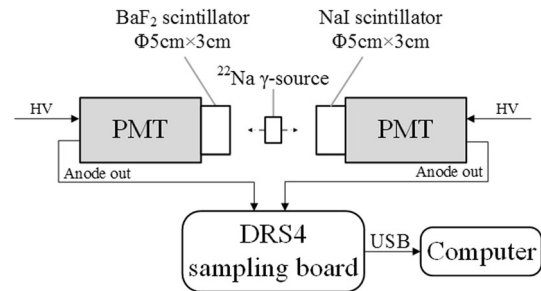


Fig. 3 Schematic diagram of the experimental setup

used the internal natural radioactivity to calibrate digital pulse sampling and  $\alpha/\gamma$  discrimination algorithms and to determine the discrimination threshold. Only the BaF<sub>2</sub> detector was used in this part.

After extracting the pulse information, the results are presented in a 2-D scatter plot of the variables corresponded to each PSD algorithm, as shown in Fig. 4. Figure 4a shows the scatter plot of the CCM algorithm. The short integrals for 170,000 events plotted against the long integrals:  $\gamma$ -rays are identified as points above the discrimination threshold (the black solid line), while  $\alpha$ -particles are identified as points lay below it. Figure 4b and c shows scatter plots of PPA and PGA. Particularly, in Fig. 4d, for the FCM algorithm, with the FIR peak ratio being in the ordinate and the ratio of short integral/long integral in the abscissa,  $\gamma$ -rays are identified as points below the discrimination threshold, while  $\alpha$ -particles are identified as points above it. Furthermore, to evaluate the separation of  $\gamma$ -ray and  $\alpha$ -particle regions, in Fig. 5 the identification spectra are obtained by calculating the distance to the discrimination threshold line in the scatter plots for each event. The spectra are fitted with Gauss function shown as the red curves, and the full width at half maximum (FWHM) of the  $\gamma$ -peak as well as the  $\alpha$ -peak in the spectra is compared in Table 1. More intuitively, figure-of-merit (FOM) values for the four methods can be calculated by Eq. (1), as shown in Table 1

$$FOM = \frac{Peak_{\gamma} - Peak_{\alpha}}{FWHM_{\gamma} + FWHM_{\alpha}} \quad (1)$$

#### 3.3 Results: <sup>22</sup>Na $\gamma$ -source

Due to the two-photon radiation of <sup>22</sup>Na, the coincidence events of BaF<sub>2</sub> detector and NaI detector can be identified as  $\gamma$ -ray events except for  $\alpha$ -induced random coincidence events. Figure 6 shows distribution histograms of the distances to the discrimination threshold line of 20,000 coincidence events from BaF<sub>2</sub> detector, corresponding to each of the four PSD algorithms. Most of the

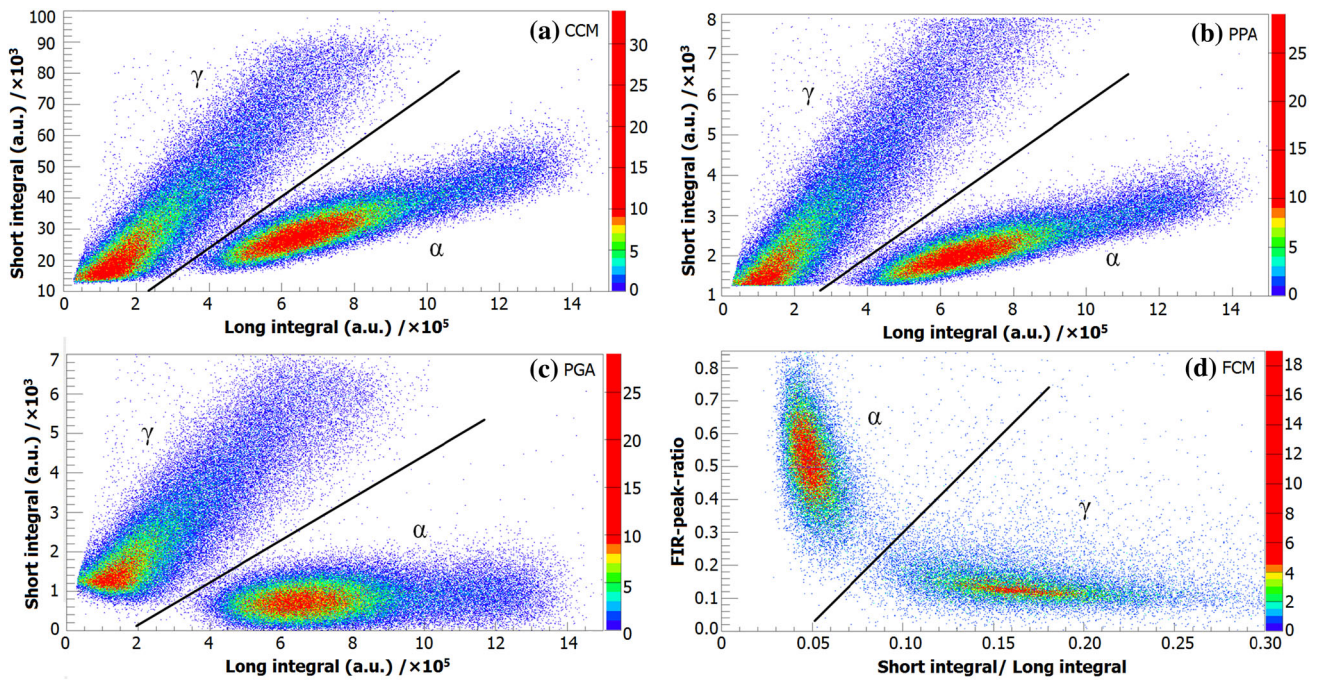


**Fig. 4** Scatter plots of the PSD algorithms. The *black solid line* indicates the discriminate threshold between  $\gamma$ -rays and  $\alpha$ -particles

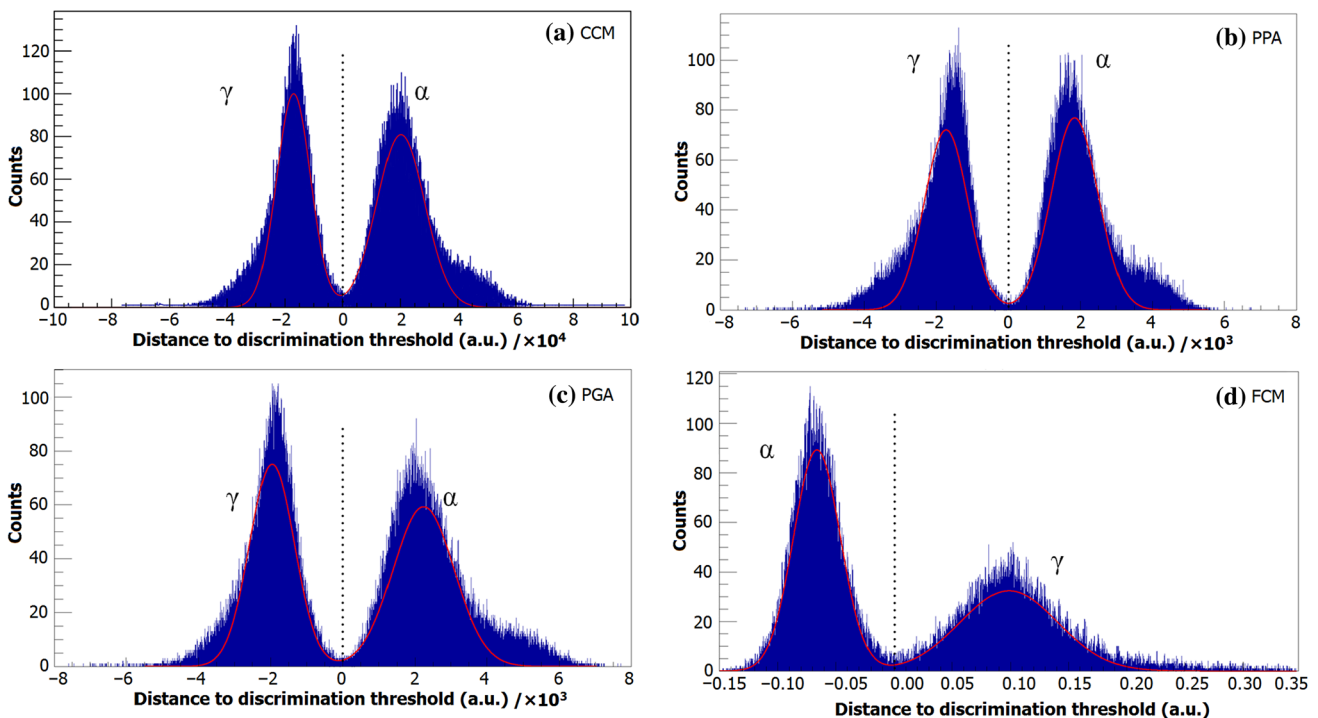


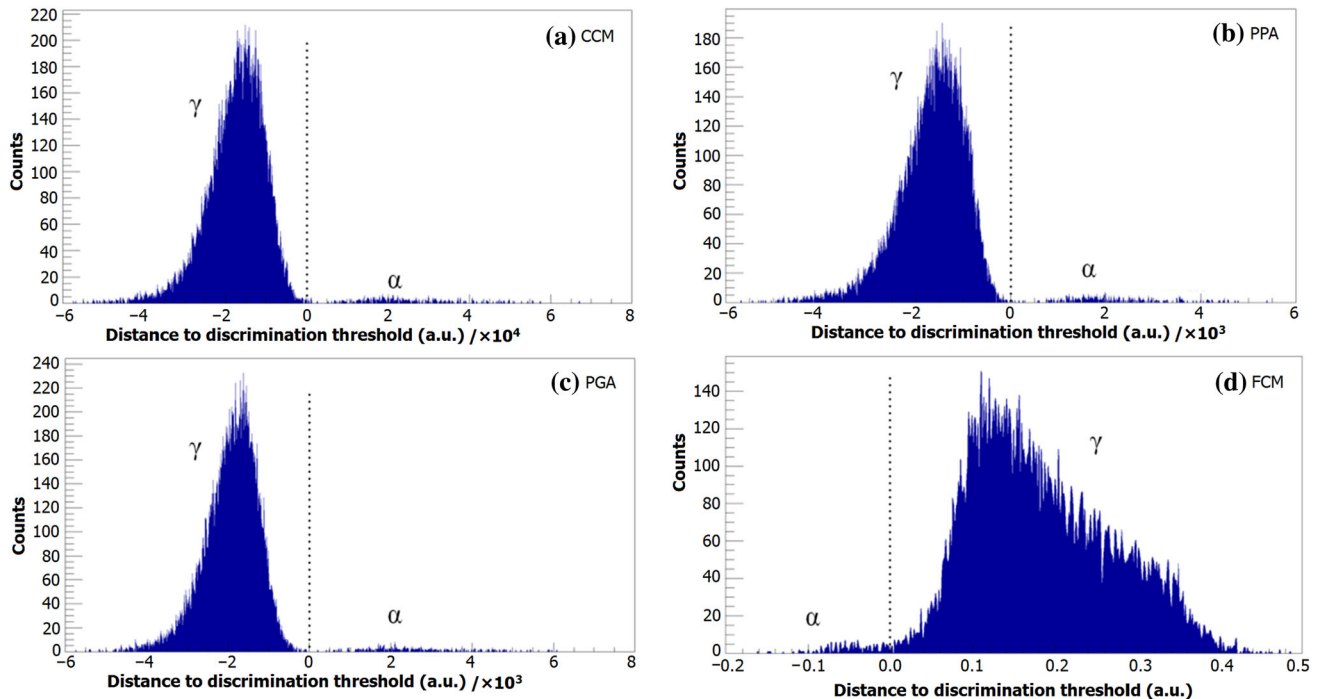
**Fig. 5** Identifying the spectra by distance from the discrimination threshold using the PSD algorithms. The *red curves* are Gauss fitting results. (Color figure online)

coincidence events are identified as  $\gamma$ -rays for all algorithms. False alarm rate (FAR) is defined as the proportion of coincidence events identified as  $\alpha$ -particles, including

$\alpha$ -induced random coincidences and wrong results of corresponding algorithms. The FARs of each algorithm are shown in Table 1.

**Table 1** Comparison of four PSD algorithms

Methods	FWHM <sub><math>\gamma</math></sub>	FWHM <sub><math>\alpha</math></sub>	Peak <sub><math>\gamma</math></sub> – Peak <sub><math>\alpha</math></sub>	FOM	FAR (%)
CCM	$1.39 \times 10^4$	$1.95 \times 10^4$	37,180	1.113	1.359
PPA	$1.43 \times 10^3$	$1.53 \times 10^3$	3568	1.205	1.339
PGA	$1.46 \times 10^3$	$2.00 \times 10^3$	4201	1.216	1.324
FCM	$4.76 \times 10^{-2}$	$9.89 \times 10^{-2}$	0.1651	1.127	1.526

**Fig. 6** Distribution histograms of the distances to discrimination threshold of coincidence events, using the PSD algorithms

### 3.4 Method comparison

Performance of the four PSD algorithms is compared in Table 1. Little variations are seen in the FOMs and FARs of the algorithms. FOM indicates the performance of separation, and the PPA and PGA algorithms are slightly better than the other two. According to the consistency of FARs for different algorithms, most of the misidentified events likely belong to  $\alpha$ -induced random coincidence events, being a fixed proportion among the whole events.

FPGA resource occupancy is also a considerable issue. With the Xilinx Spartan-3 family (XC3S5000) FPGA, for CCM, PPA and PGA algorithms, 10% LUTs (6831 of 66,560) and 13% slices (4389 of 33,280) were used. And for FCM algorithm, due to the use of the FIR filter, 59% LUTs (39,545 of 66,560) and 85% slices (28,618 of 33,280) were used. Except for FCM algorithm, other algorithms show small FPGA resource utilization, considering that Spartan-3 family FPGA is low cost and has small chip size.

In summary, FCM achieves similar performance but costs much more FPGA logical resources than the other algorithms. Comprehensively, considering the performance and FPGA usage, PGA turns out the best of all the four algorithms.

## 4 Discussion

Pulse information extraction is the key technique of the PSD algorithms. The good separations of  $\alpha/\gamma$  events in identification spectra of each algorithm are mainly based on the information extracted in FPGA, well presenting notable features of different pulses. Besides, the extraction executed in FPGA greatly compresses the packet size, hence the reduced transmission time, shortened dead time and reduced usage of FPGA logical resources.

The events type can be judged in FPGA after obtaining the discrimination thresholds, instead of after transmitting to computer. Using several multiplier–adders and comparators after pulse information extraction, the real-time

PSD can be achieved. With the good performance, very short dead time and low logical resource usage, it is prospective to use PSD algorithms like PGA in future BaF<sub>2</sub> detector experiments, such as CSNS-WNS (white neutron source at China Spallation Neutron Source) [15, 16], to discriminate  $\alpha/\gamma$  events and eliminate  $\alpha$ -background.

## 5 Conclusion

Four FPGA-based digital PSD algorithms were investigated and compared in this work; similar PSD performance was observed in BaF<sub>2</sub> detector. Besides, based on the pulse information extraction technique, the dead time and logical resource cost are significantly reduced, which makes the PSD algorithms suitable for real-time pulse processing in high-rate field experiments.

**Acknowledgements** The authors would thank Prof. Stefan Ritt and Dr. Jinhong Wang for their help.

## References

1. M. Laval, M. Moszyński, R. Allemand et al., Barium fluoride— inorganic scintillator for subnanosecond timing. *J Nucl. Instrum. Methods Phys. Res.* **206**, 169–176 (1983). doi:[10.1016/0167-5087\(83\)91254-1](https://doi.org/10.1016/0167-5087(83)91254-1)
2. F. Amorini, E. De Filippo, P. Guazzoni et al., Digital pulse shape acquisition from BaF<sub>2</sub>: preliminary results. Paper presented at the 2006 IEEE nuclear science symposium conference record, IEEE, San Diego, 29 Oct–1 Nov 2006
3. R. Novotny, Performance of the BaF<sub>2</sub>-calorimeter TAPS. *J. Nucl. Phys. B Proc. Suppl.* **61**, 137–142 (1998). doi:[10.1016/S0920-5632\(97\)00552-5](https://doi.org/10.1016/S0920-5632(97)00552-5)
4. K. Wisshak, F. Käppeler, Large barium fluoride detectors. *J. Nucl. Instrum. Methods Phys. Res. Sect. A Accel. Spectrom. Detect. Assoc. Equip.* **227**, 91–96 (1984). doi:[10.1016/0168-9002\(84\)90105-0](https://doi.org/10.1016/0168-9002(84)90105-0)
5. E. Dafni, A note on the application of BaF<sub>2</sub> scintillators to  $\gamma$ -ray and charged particle detection. *J. Nucl. Instrum. Methods Phys. Res. Sect. A Accel. Spectrom. Detect. Assoc. Equip.* **254**, 54–60 (1987). doi:[10.1016/0168-9002\(87\)90481-5](https://doi.org/10.1016/0168-9002(87)90481-5)
6. E. De Filippo, G. Lanzanó, A. Pagano et al., A study of light quenching in BaF<sub>2</sub> crystals for heavy ions at intermediate energies. *J. Nucl. Instrum. Methods Phys. Res. Sect. A Accel. Spectrom. Detect. Assoc. Equip.* **342**, 527–533 (1994). doi:[10.1016/0168-9002\(94\)90282-8](https://doi.org/10.1016/0168-9002(94)90282-8)
7. G. Lanzanó, A. Pagano, S. Urso et al., Using BaF<sub>2</sub> crystals as detectors of light charged particles at intermediate energies. *J. Nucl. Instrum. Methods Phys. Res. Sect. A Accel. Spectrom. Detect. Assoc. Equip.* **312**, 515–520 (1992). doi:[10.1016/0168-9002\(92\)90199-E](https://doi.org/10.1016/0168-9002(92)90199-E)
8. J. Gál, G. Kalinka, B.M. Nyakó et al., Particle discriminator for the identification of light charged particles with CsI (TI) scintillator + PIN photodiode detector. *J. Nucl. Instrum. Methods Phys. Res. Sect. A Accel. Spectrom. Detect. Assoc. Equip.* **366**, 120–128 (1995). doi:[10.1016/0168-9002\(95\)00560-9](https://doi.org/10.1016/0168-9002(95)00560-9)
9. R. Aryaeinejad, J.K. Hartwell, D.F. Spencer, Comparison between digital and analog pulse shape discrimination techniques for neutron and gamma ray separation. Paper presented at the 2005 IEEE nuclear science symposium conference record, IEEE, Fajardo, 23–29 Oct 2005
10. J.M. Adams, G. White, A versatile pulse shape discriminator for charged particle separation and its application to fast neutron time-of-flight spectroscopy. *J. Nuclear Instrum. Methods* **156**, 459–476 (1978). doi:[10.1016/0029-554X\(78\)90746-2](https://doi.org/10.1016/0029-554X(78)90746-2)
11. B. D'Mellow, M.D. Aspinall, R.O. Mackin et al., Digital discrimination of neutrons and  $\gamma$ -rays in liquid scintillators using pulse gradient analysis. *J. Nucl. Instrum. Methods Phys. Res. Sect. A Accel. Spectrom. Detect. Assoc. Equip.* **578**, 191–197 (2007). doi:[10.1016/j.nima.2007.04.174](https://doi.org/10.1016/j.nima.2007.04.174)
12. S. Ritt, Design and performance of the 6 GHz waveform digitizing chip DRS4. Paper presented at the 2008 IEEE nuclear science symposium conference record, IEEE, Dresden, 19–25 Oct 2008
13. J.H. Wang, L. Zhao, C.Q. Feng et al., Evaluation of a fast pulse sampling module with switched-capacitor arrays. *J. IEEE Trans. Nucl. Sci.* **59**, 2435–2443 (2012). doi:[10.1109/TNS.2012.2208656](https://doi.org/10.1109/TNS.2012.2208656)
14. Xilinx, Spartan-3 FPGA Family Data Sheet (Xilinx Inc, 2013). [http://www.xilinx.com/support/documentation/data\\_sheets/ds099.pdf](http://www.xilinx.com/support/documentation/data_sheets/ds099.pdf). Accessed 15 Aug 2016
15. J.Y. Tang, S.N. Fu, H.T. Jing et al., *J. Chin. Phys. C* **34**, 121 (2010)
16. B. He, P. Cao, D.L. Zhang et al., Clock distributing for BaF<sub>2</sub> readout electronics at CSNS-WNS. [arXiv:1602.06635](https://arxiv.org/abs/1602.06635) [physics.ins-det]